Photonic Crystals and Plasmonic Structures Recorded by Multi-Exposure of Holographic Patterns

Jacson W. Menezes[a] Edmundo S. Braga[a] and Lucila Cescato[b]
[a]Faculdade de Engenharia Elétrica e Computação, Unicamp
[b]Instituto de Física Gleb Wataghin, Unicamp, Campinas Brasil CEP 13083-970

ABSTRACT

Different technologies can be used for fabrication of photonic crystals such as: self-assembly of colloidal particles, e-beam lithography (EB), interference lithography (IL) and focused ion beam (FIB). Among them, the holographic lithography (HL) is the only technique that is able to fabricate both two-dimensional and three-dimensional photonic crystals, as well as plasmonic structures, in large areas. In this paper we demonstrate the use of the multi-exposure of two-beam interference patterns, with rotation of the sample around different axis, for fabrication of large areas 2D and 3 D photonic crystals and plasmonic structures. Using this technique, we achieved aspect ratios of about 4 in 2D photoresist templates recorded in 1 cm^2 glass substrates. In order to generate the 2D photonic band gap layers and plasmonic structures, we combine the use the high aspect ratio photoresist templates with shadow evaporation of appropriated materials, with a further lift-off of the photoresist. The optical properties of the recorded structures, both photonic and plasmonic, were measured to demonstrate the applicability of the technique.

Keywords: Photonic Crystal, Plasmonics, Holographic Lithography

1. INTRODUCTION

Photonic Crystals (PC) and Plasmonic Structures have attracted growing interest because of their ability to mold the light behavior and thus to generate new type of applications [1-4].

Two dimensional photonic crystal (2D PC) layers have been extensively demonstrated in the last years. They can be fabricated by Electron Beam Lithography (EBL) [2], Focused Ion Beam (FIB) [5] or Interference Lithography (IL)[6]. By the other hand, three-dimensional Photonic Crystal (3D PC) templates can be fabricated by self-arrangement of colloidal particles [7], direct laser writing [8] or holographic lithography [9-10]. Plasmonic structures are mostly fabricated by FIB[3,4]. Among these fabrication techniques, the holographic lithography is the only one that is able to fabricate either 2D or 3D Photonic Crystal templates, as well as plasmonic structures, in large areas.

The holography fabrication of 3D PC employs generally a single exposure of multiple beams [9,10]. Such method, however, reduces the contrast of fringe pattern as well as the exposure area. An alternative way is the multi-exposure of two beam interference patterns, with rotation of the sample between the exposures [11,12], instead of a single exposure of multiple beams. Multiple exposures present some advantages: the two interfering beams may have the same polarization and it is possible to set up very stable two-beam interferometers for generation of high quality fringe patterns in large areas [12]. Such advantages result in higher contrast of the intensity light pattern allowing the recording of well-defined homogeneous structures in large areas.

In this paper, we demonstrate the use of the multiple exposures of two beam interference patterns to fabricate, 2D and 3 D photonic crystals templates as well as plasmonic structures.

Holography: Advances and Modern Trends, edited by Miroslav Miler, Miroslav Hrabovský,
Proc. of SPIE Vol. 7358, 73580K · © 2009 SPIE · CCC code: 0277-786X/09/$18 · doi: 10.1117/12.820136

2. SIMULATED LIGHT PATTERNS

If we expose a photosensitive material to several two-beam interference patterns, the resulting light dose inside the photosensitive material is the sum of the light intensity I_{Ri} of each interference fringe pattern multiplied by the time of each exposure (Δt_i).

$$E_R = \sum_{i=1}^{n} (\Delta t_i) I_{Ri} \tag{1}$$

Assuming that each fringe pattern is formed by two linearly parallel polarized plane wave-fronts with equal irradiance, forming an angle 2θ between them (Figure 1), the irradiance I_{Ri} of each interference pattern inside the photosensitive material can be expressed by:

$$I_{R1} = 2I(1 + Cos(\vec{k}_1 \cdot \vec{r} - \vec{k}_2 \cdot \vec{r})) \tag{2}$$

with $\vec{k}_1$ and $\vec{k}_2$ given by:

$$\vec{k}_1 = \left[-\frac{2\pi n_r}{\lambda} \right] \left(Sin(\xi)Cos(\alpha)\hat{i} + Cos(\xi)\hat{j} + Sin(\xi)Sin(\alpha)\hat{k} \right) \tag{3}$$

$$\vec{k}_2 = \left[\frac{2\pi n_r}{\lambda} \right] \left(Sin(\rho)Cos(\alpha)\hat{i} - Cos(\rho)\hat{j} + Sin(\rho)Sin(\alpha)\hat{k} \right) \tag{4}$$

with α being the rotation angle of the sample around y axis (Figure 1). In this equation n_r is the refractive index of the photosensitive material, ρ and ξ are the angles formed between each incident beam and the normal to the substrate, inside the material. Such angles are related with the angle 2θ formed between the incident beams (in air) and the rotation angle of the sample β (around the z axis) by the Snell law:

$$\xi = ArcSin\left[\frac{1}{n_r} Sin(\theta + \beta) \right] \tag{5}$$

$$\rho = ArcSin\left[\frac{1}{n_r} Sin(\theta - \beta) \right] \tag{6}$$

By assuming an equal and constant irradiance in both interfering waves inside the photosensitive material, we are neglecting the variation of the light intensity with the incident angle and the absorption of the photosensitive material. Both assumptions are reasonable for our experimental conditions because: a) we use as a light source a blue laser (458nm) for which the absorption of the photosensitive material (positive photoresist) is very low and b) the variation of the reflectance with the incident angle do not change significantly the contrast of the fringe pattern, but it only reduces the total light intensity (I) of the interference pattern, inside the material, of about 10%, for the maximum angles that we can use in our setup. The increasing of the exposure time can compensate this variation, but it does not affect the geometry of the recorded structures.

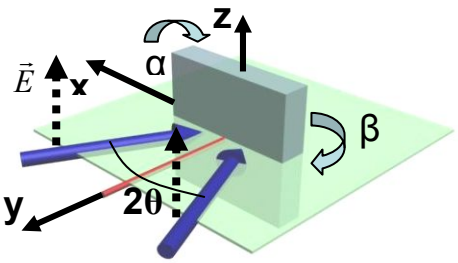

Fig. 1. Scheme of the incident beams and rotation angles of the sample α and β, around the axis y and z respectively.

2.1 Two dimensional layer

If the normal to sample is aligned with the bisector of the two incident beams (y axis), that means $\beta=0^o$ and we expose the sample twice to the same interference pattern by rotating the sample around the y-axis of $\alpha_1=45^o$ and $\alpha_2=-45^o$ (or $\alpha_1=0^o$ and $\alpha_2=90^o$) for each exposure respectively, a squared lattice will be recorded [6]. By other hand if we rotate the sample around the same y-axis of $\alpha_1=30^o$ and $\alpha_2=-30^o$ (or $\alpha_1=0^o$ and $\alpha_2=60^o$) for each exposure respectively, a hexagonal lattice will be recorded [12,13]. In such case, the irradiance I_{Ri} of each interference pattern inside the photosensitive material can be simplified by:

$$I_{Ri} = 2I\left\{1+\cos\left[\frac{2\pi}{\Lambda_i}\left(\cos(\alpha_i)x-\sin(\alpha_i)z\right)\right]\right\} \tag{7}$$

with $\Lambda_i=\lambda/2\mathrm{Sin}\theta$ being the period of the fringe pattern.

Figure 2 shows the simulated light patterns that correspond to the surfaces of equal energy dose value of equation (1). Figure 2(a) corresponds to a superimposition of two sinusoidal fringe patterns with the rotation angle of the sample $\alpha_1=45^o$ and $\alpha_2=-45^o$ for the first and second exposure respectively. Figure 2(b) shows the same for $\alpha_1=0^o$ and $\alpha_2=-60^o$. In both cases the period of fringe pattern was kept constant and equal to $\Lambda_1=\Lambda_2=0.7\mu m$ as well as the time of exposure of each pattern ($\Delta t_1=\Delta t_2$).

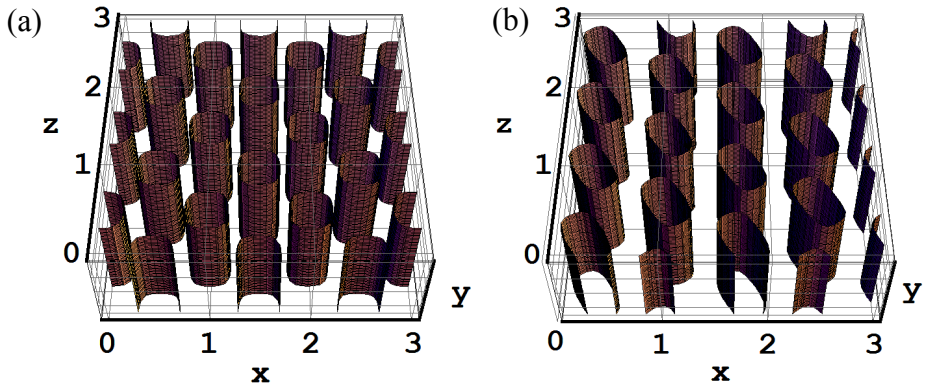

Fig. 2. Simulated light patterns (surface of equal energy dose) resulting from the superimposition of two interference patterns. The sample was rotated of a) $\alpha_1=45^o$ and $\alpha_2=-45^o$ and b) $\alpha_1=0^o$ and $\alpha_2=-60^o$.

The hexagonal structure obtained by a rotation of the sample of 60^o between the exposures (Figure 2b), presents an elliptical cross section [12,13]. Adding a third exposure can eliminate such ellipticity. In this case, however, it is necessary to control the phase-shift between the third exposure and the former two [14].

2.2 Two dimensional infinite channels

In this case we expose the sample twice to the same interference pattern but now we rotated the sample around z-axis, instead of y-axis (α=0). Using $\beta_1 = \beta$ for the first exposure and $\beta_2 = -\beta$ for the second exposure, the resulting interference pattern can be written by:

$$I_{Ri} = 2I\left\{1+\cos\left[-\frac{2\pi n_r}{\lambda}\left([\sin(\xi)+\sin(\rho)]x+[\cos(\xi)-\cos(\rho)]y\right)\right]\right\} \qquad (8)$$

with ξ and ρ given by equations 5 and 6.

Figure 3(a) shows the simulated light pattern inside the photoresist film resulting from the superimposition of two sinusoidal fringe patterns with de same period $(\Lambda_1=\Lambda_2=0.7\mu m)$ and same time of exposure $\Delta t_1=\Delta t_2$. The refractive index of the photosensitive material was assumed $n_r=1.67$ and the rotation angles of the sample were $\beta_1=+45^o$ and $\beta_2=-45^o$ for each exposure respectively. As it can be seen in Figures 3(a) the superimposed pattern is a hexagonal array of tubes, aligned with the z-axis (parallel to substrate surface), with elliptical cross section (Figure 3(c)). Figure 3(b) shows the light pattern simulation for $\beta_1=+15^o$ and $\beta_2=-15^o$, while Figure 3 (d) corresponds to its cross-section at plane x-y.

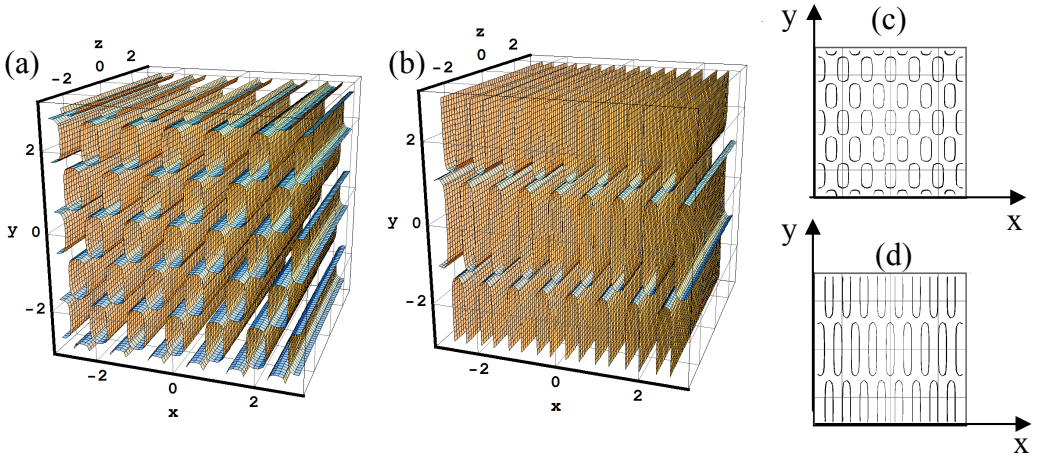

Fig. 3. Simulated light patterns for rotation of the sample around z-axis of angles (a) $\beta_1=+45^o$ and $\beta_2=-45^o$; (b) $\beta_1=+15^o$ and $\beta_2=-15^o$. (c) and (d) are the x-y cross-sections of (a) and (b) respectively.

2.3 Three-dimensional

By superimposing three interference patterns with rotation of the sample around both y and z-axis of proper angles α and β it is possible to generate 3D photonic crystal templates [11]. Different kinds of 3D periodic structures can be simulated (using equations 1 to 6) and it is possible to find the appropriate conditions to perform the holographic recording of the desired structure. Figure 5(a) shows the simulated pattern resulting from the superimposition of three fringe patterns with the rotation angles of the sample of $\alpha_1=90^o$; $\beta_1=0^o$, for the first exposure, $\alpha_2=0^o$, $\beta_2=30^o$, for the second exposure and $\alpha_3=0^o$, $\beta_3=-30^o$ for the third exposure. As it can be observed, the 3D simulated structures present a squared lattice in the plane x-z, a hexagonal lattice in the planes x-y and a rectangular lattice in the plane z-y. Figures 5 (b), (c) and (d) correspond to the cross-sections of the Figure 5(a).

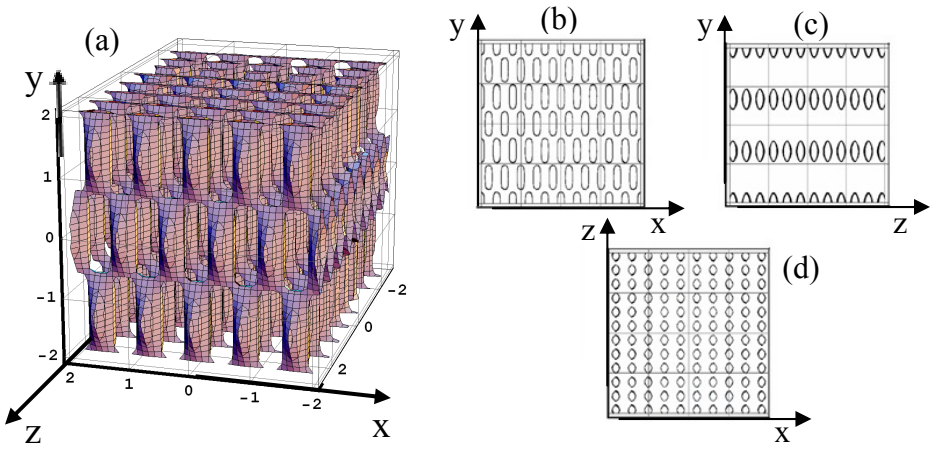

Fig. 4. Simulated light patterns resulting from the superimposition of three interference patterns for rotation angles of the sample: α_1=90°, β_1= 0°; α_2=0°, β_2= 30° and α_3=0°, β_3= -30°. (b), (c) and (d) correspond to the cross sections at planes y-x, z-y and z-x respectively.

3. RECORDING OF THE PHOTORESIST TEMPLATES

In order to record the conventional structures, the positive photoresist SC 1827 (from Rohm and Haas) was spin-coated on glass substrates forming a 0.6 μm thick film. The samples were pre-baked and then exposed twice to a stabilized holographic setup [15] operating at λ = 458nm. We have used a fringe period of 0.7μm and a dose of 350 mJ/cm^2 in each exposure. The samples were exposed using the same rotations α angles used in the simulations of Figure 2. After the second exposure, the sample is developed in AZ 351 developer 1:4 for about 40 seconds.

Figure 5 (a) shows the SEM-photographs of the photoresist structures, recorded using α_1 =45 ° and α_2 =-45 ° while Figure 5 (b) shows the same for α_1 =0 ° and α_2 =-60 °. Note the good accordance between the experimental and simulated structures (Figure 2). The photoresist template is constituted of well-defined columns, measuring around 0.6 μm of high, resulting in aspect ratio of about 4, and an average filling factor around 0.2. The lateral walls of the structures are verticals, which is a necessary characteristic for the lift-off process.

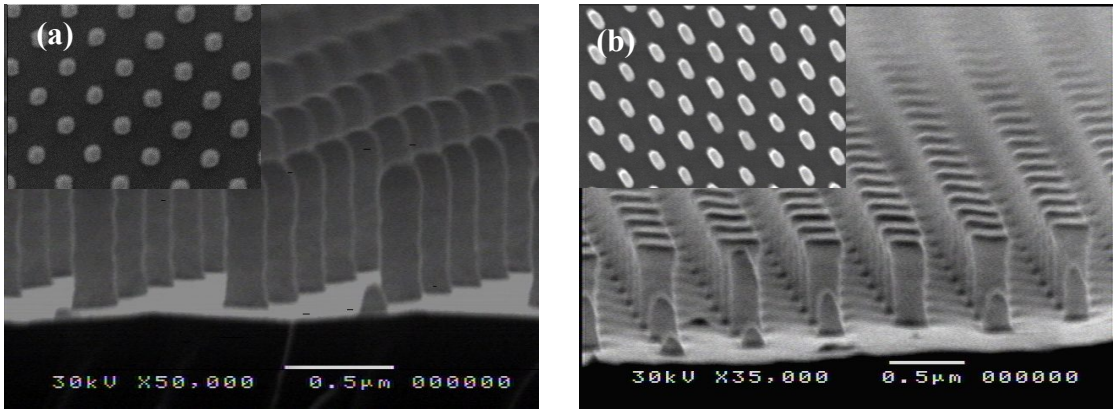

Fig. 5. SEM photographs of the SC 1827 photoresist templates on glass substrate a) α_1= + 45 ° and α_2 = - 45 °; (b) α_1= 0 ° and α_2 = -60 ° resulting in a 2D squared and 2D hexagonal lattice respectively.

To record the "infinite" channels structures, thick photoresist films, of AZ 1518 (from Hochst), were prepared with a thickness of about 8 μm. The samples are exposed twice to the same holographic setup [15] but now the samples were rotated around the z axis, of symmetrical angles β=±45° and β=±15°, and the light dose of each exposure was 600 mJ/cm^2. After the second exposure, the samples were developed in AZ 351 developer 1:3 for about 45 seconds. Figure 6

shows the SEM-photographs of the cross section of the photoresist structures, recorded with these two different β angles. The resulting structure is composed by a hexagonal arrays of "infinite" channels with their axis aligned along the substrate surface. Note the good accordance between the experimental and simulated patterns (shown in Figure 3). The "infinite" channels shown in Figure 6 can be observed along the whole sample that has about 1cm^2.

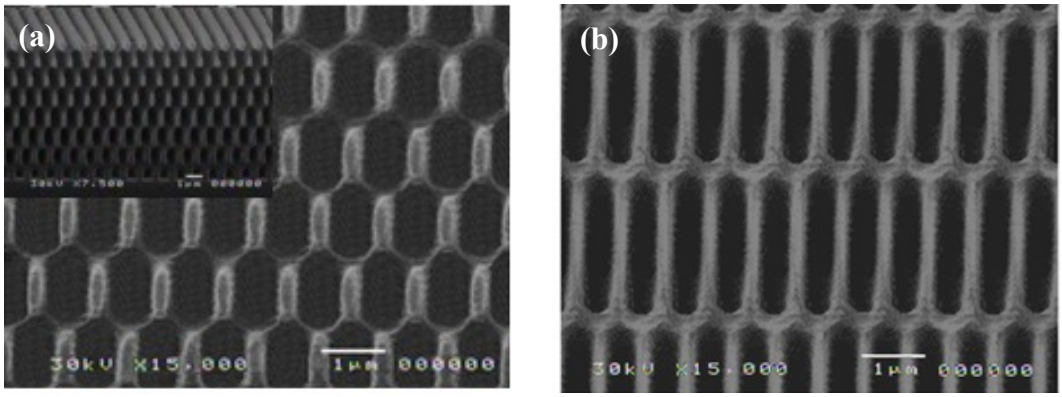

Fig. 6. SEM-photographs of the cross section of the structures recorded in photoresist by superimposition of patterns by rotating the sample around the z-axis. (a) $\beta_1 = +45^o$ and $\beta_2 = -45^o$; (b)) $\beta_1 = +15^o$ and $\beta_2 = -15^o$. The inset in (a) shows an overview of the sample.

The same thick AZ 1518 photoresist film was used to record the 3D structures. In this case, at least three exposures are necessary, with rotation of the sample around different axis. Figure 7 shows the structure resulting from three successive exposures of the sample to the same interference fringe pattern. For the first exposure we used $\alpha_1 = 90^o$; $\beta_1 = 0^o$, for the second exposure, $\alpha_2 = 0^o$, $\beta_2 = 30^o$, and for the third exposure $\alpha_3 = 0^o$, $\beta_3 = -30^o$. The inset corresponds to the top view of the sample (cross-section at the plane z-x). As expected, the photoresist template is a three-dimensional lattice with squared lattice at the plane z-x (top view inset) and a hexagonal lattice at the plane y-x. Besides the effect of the absorption that changes the width of the photoresist structures along the y-axis, there is a good agreement between the photoresist cross-section and the simulated cross-section.

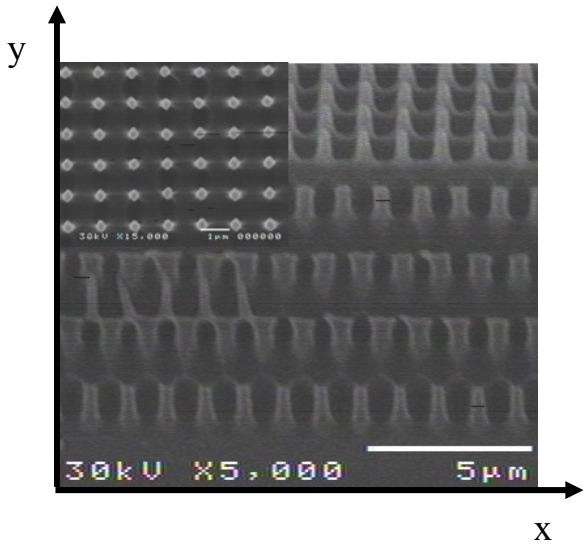

Fig. 7. Scanning electro photography of the 3D photoresist template recorded using three exposures: $\alpha_1 = 90^o$; $\beta_1 = 0^o$, for the first exposure, $\alpha_2 = 0^o$, $\beta_2 = 30^o$, for the second and $\alpha_3 = 0^o$, $\beta_3 = -30^o$ for the third. The inset shows a top view of the sample (plane z-x).

4. PHOTONIC AND PLASMONIC STRUCTURES

The 2D photoresist templates can be used to transfer the pattern to a dielectric with high refractive index material, in order to present photonic band gap (PBG) in all direction of propagations, in the plane.

The transference of the pattern was performed using the shadow evaporation of the desired dielectric material. As the photoresist templates present a high aspect ratio, with vertical walls, the evaporated material coats only the top and the bottom of the photoresist structure, keeping the photoresist lateral walls bared. Thus, after evaporation the photoresist is removed using a lift-off with acetone. Figure 8 shows these three steps: (a) the photoresist template on the glass substrate; (b) the sample after the evaporation of the antimony based glass film (with refractive index of about 1.9) and (c) after the photoresist lift-off in acetone [16]. The resulting hexagonal 2D photonic crystal layer has a thickness of 200 nm, a hexagonal lattice period a= 808 nm and a filling factor r/a =0.37 [16].

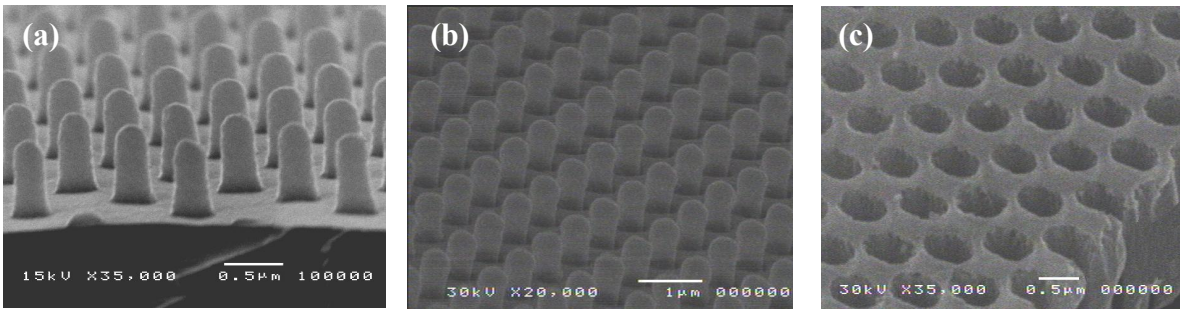

Fig. 8. Scanning Electron photographs of the three steps of the process (a) photoresist template; (b) after the antimony based glass deposition and (c) patterned antimony based glass layer, after lift-off of photoresist.

In order to obtain the plasmonic structures, the pattern must be transferred to a metallic film. Figure 9(a) shows the SEM photograph of the resulting 2D squared arrays of holes recorded by e-beam evaporation of Au and further lift-off of the photoresist. The holes have diameter of 150nm, period of 700nm and the thickness of the Au film is about 100nm. The samples are about 1 inch squared and are homogeneous along this whole area. Figure 9 (b) shows the SEM photograph of the hexagonal array of nanoholes recorded in Au films with the same thickness (100 nm). In this case the period of the fringe pattern used was 800 nm resulting in a period of 900 nm for the hexagonal lattice. The elliptical holes measure about 200 nm X 400 nm (minor X major axis).

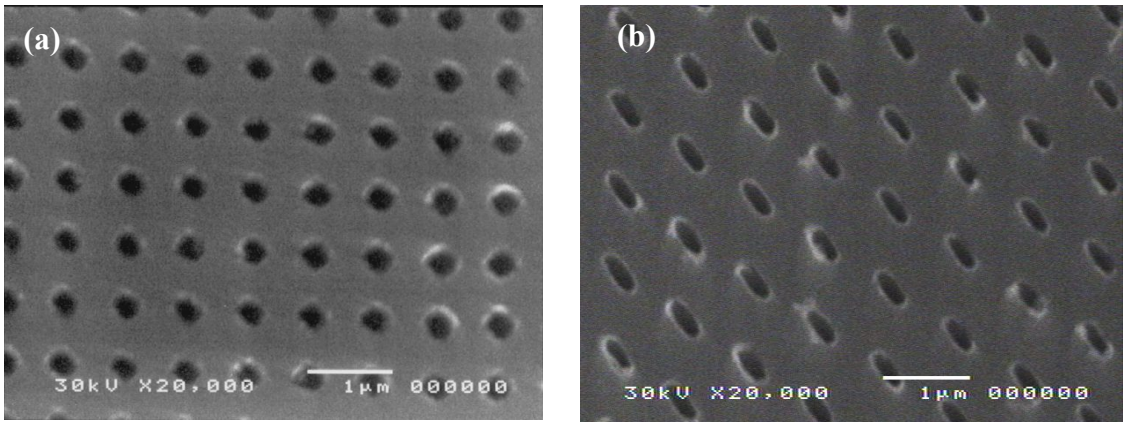

Fig. 9. Scanning electron photographs of the arrays of holes in Au films of 100nm of thickness: (a) Squared lattice and (b) Hexagonal lattice

5. OPTICAL MEASUREMENTS

In order to check the applicability of this technique to perform photonic crystals, the photonic properties of the recorded samples were measured by optical transmittance spectroscopy.

Figure 10 shows the optical transmission spectrum of the 2D patterned antimony based glass layer (shown in Figure 8 (c)) as a function of incidence angle θ along the direction Γ-K (schematized in Figure 10). The measurements were performed in two different regions of the sample, separated from each other of about 5 mm, using a Cary 500 Spectrometer from Perkin Elmer in the range from 650 to 2000 nm for the incident light linearly polarized along the TE direction (perpendicular to the plane of incidence). The transmittance curves display the resonant features (Fano ressonances) when the frequency and the component of the wavevector parallel to the surface matches a photonic mode in the layer [17]. Note that the resonances peaks are as well defined as those obtained from samples fabricated by e-beam or FIB [17]. This fact indicates that there is no substantial variation of the geometric parameters of the holes in the spot size area of the measurement (~3.5mm^2). Note also that there is no significant variation between the spectra for two different regions that demonstrates the good homogeneity of the sample.

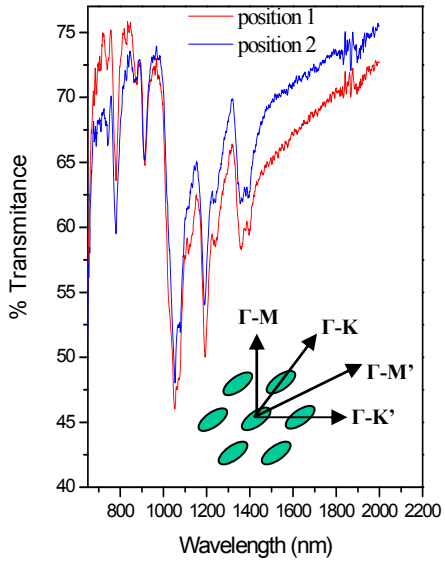

Fig. 10. Transmission spectra obtained for the 2D-PCL sample by changing the incidence angle. Measurements were done along the Γ-K direction, for TE polarization.

Figure 11(a) shows the zero-order transmission spectra, measured using a λ-9 Perkin Elmer Spectrometer (VIS-UV), for a squared array of holes in a gold film on a glass substrate (sample of Figure 9 (a)). Each color corresponds to a different point of the sample separated each other of about 5mm. As it can be seen the spectra do not change significantly along the sample. Figure 11 (b) shows the same transmission spectrum for the sample immersed in water. The peak at 650 nm in the Figure 11(a) is related to the Au-air (n=1) interface, while the peak at 725 nm in Figure 11(b) is related to the mode at the Au-water (n=1.332) interface. Both spectra were obtained using the same sample and they are superimposed in Figure 11(c), for comparison. The SP modes are distinctly different because the resonance frequency depends on the dielectric constant of the local medium [3,4]. Note that the position of the first peak (λ=495nm) is the same for the sample immersed both in air and in water.

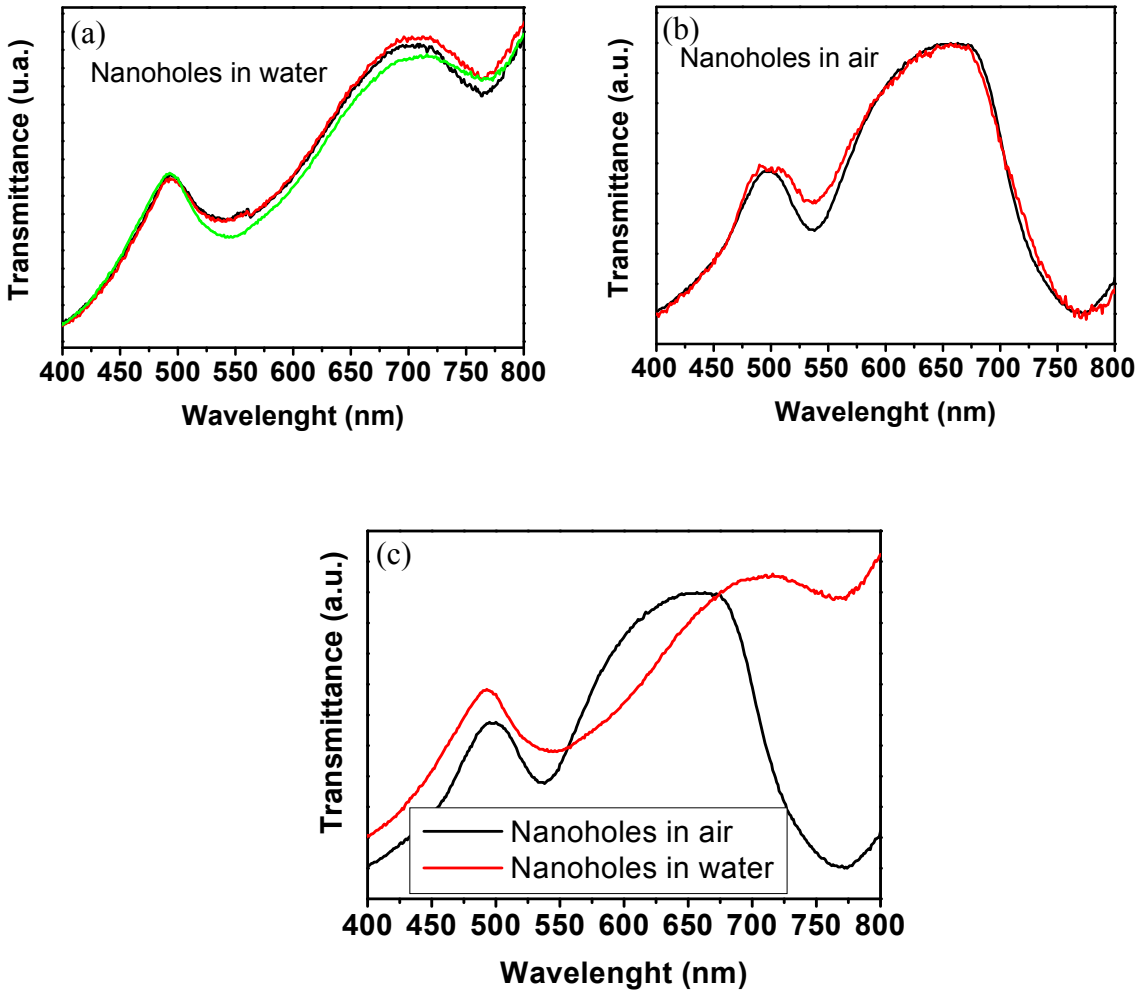

Fig. 11. Optical transmission spectra of the squared array of holes recorded in a gold film with 100nm of thickness (shown in Figure 9 (a)). Each color corresponds to a different point of the sample. (a) Sample immersed in air; (b) Sample immersed in water and (c) Superposition of the curves for comparison.

6. CONCLUSIONS

We demonstrated the fabrication of 2D and 3D photonic crystals and plasmonic structures using the superimposition of two-beam interference patterns.

To record 2D photonic crystal layers as well as plasmonic structures only two exposures are enough to obtain high aspect ratio photoresist templates. These templates are used to transfer the pattern to appropriate materials by lift-off. The optical measurement of the samples fabricated using this method shows the presence of Fano and plasmonic resonance peaks that demonstrates the applicability of the technique.

For recording of 3D photonic structures three exposures are necessary, at least. In this case the maximum thickness of the 3D PC templates is limited by the photoresist absorption and by the mechanical properties of the photoresist.

ACKNOWLEGMENTS

We acknowledge the financial support from the Fundação de Amparo a Pesquisa do Estado de São Paulo (FAPESP) and Conselho Nacional de Pesquisa (CNPq).

REFERENCES

[1] Joannopoulos, J. D., Meade, R. D. and Winn, J. N., *Photonic Crystals* (Princeton University Press, 1995).

[2] Notomi, M., Shinya, A. and Kuramochi, E., "Photonic crystals: Towards ultrasmall lightwave circuits," NTT Tech. Rev. 2, 36-47 (2004).

[3] Ebbesen, T. W., Lezec, H. J., Ghaemy, H. F., Thio, T. and Wolff, P. A., "Extraordinary optical transmission through sub-wavelenght hole arrays," Nature, 391, 667-669 (1998).

[4] Gordon, R., Sinton, D., Kavanagh, K. L. and Brolo, A. G., "A new generation of sensors based on extraordinary optical transmission," Accounts of chemical research, 41, 1049-1057 (2008).

[5] Cabrini, S., Carpentiero, A., Kumar, R., Businaro, L., Candeloro, P., Prasciolu, M., Gosparini, A., Andreani, C., De Vittorio, M., Stomeo, T., Di Fabrizio, E., "Focused ion beam lithography for two dimensional array structures for photonic applications," Microelec. Eng. 78-79, 11-15 (2005).

[6] Brueck, S. R. J., "Optical and Interferometric Lithography—Nanotechnology Enablers," Proc. IEEE 93, 1704-1721 (2005)

[7] Wijnhoven, J. E. G. J., Vos W. L., "Preparation of Photonic Crystals Made of Air Spheres in Titania," Science, 281, 802-804 (1998).

[8] Deubel, M., Freymann, G. V., Wegener, M., Pereira, S., Busch, K. and Soukoulis, C. M., "Direct laser writing of three-dimensional photonic-crystal templates for telecommunications," Nature Mater., 3, 444-447 (2004)

[9] Campbel, M., Sharp, D. N., Harrison, M. T., Denning, R. G. and Turberfield, A. J., "Fabrication of photonic crystals for the visible spectrum by holographic lithography," Nature 404, 53-56 (2000).

[10] Miklyaev, Y. V., Meisel, D. C., Blanco, A., and Von Freymann, G., "Three-dimensional face-centered-cubic photonic crystal templates by laser holography: fabrication, optical characterization, and band-structure Calculations," Appl. Phys. Lett., 82, 1284-1286 (2003)

[11] Lai, N. D., Liang, W. P., Lin, J. H., Hsu, C. C., and Lin, C. H., "Fabrication of two- and three-dimensional periodic structures by multi-exposure of two-beam interference technique," Opt. Express 13, 9605-9611 (2005).

[12] Quiñónez, F., Menezes, J. W., Rodriguez-Esquerre, V. F., Hernandez-Figueroa, H., Mansano, R. D. and Cescato, L. "Band gap of hexagonal 2D photonic crystals with elliptical holes recorded by interference lithography," Opt. Express 14, 4873-4879 (2006)

[13] Yang, X. L., Cai, L. Z. and Wang, Y. R., "Larger bandgaps of two-dimensional triangular photonic crystals fabricated by holographic lithography can be realized by recording geometry design," Opt. Express 12, 5850-5856 (2004).

[14] Menezes, J. W., Cescato, L., Carvalho, E. J. and Braga, E. S., "Recording different geometries of 2D hexagonal photonic crystals by choosing the phase between two-beam interference exposures," Opt. Express 14, 8578-8583 (2006)

[15] Frejlich, J., Cescato, L., and Mendes, G. F., "Analysis of an active stabilization system for holographic setup," Appl. Opt. 27, 1967-1976 (1988).

[16] Nalin, M., Menezes, J. W., Braga, E. S., Siu li, M., Messaddeq, Y., Ribeiro, S. J. L., Cescato, L., "2D photonic crystals in antimony-based films fabricated by holography," J. of Appl. Phys. 103, 106101-1-106101-3 (2008).

[17] Astratov, V. N., Culshaw, I. S., Stevenson, R. M., Whittaker, D. M., Skolnick, M. S., Krauss, T. F. and de la Rue, R. M., "Resonant Coupling of Near-Infrared Radiation to Photonic Band Structure Waveguides," J. Lightwave Technol. 17, 2050-2057 (1999).